Neurobiology of Disease 178 (2023) 106015

Contents lists available at ScienceDirect

Neurobiology of Disease

journal homepage: www.elsevier.com/locate/ynbdi

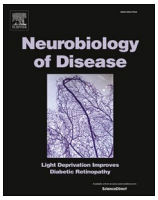

Early derangement of axonal mitochondria occurs in a mouse model of progressive but not relapsing-remitting multiple sclerosis

Daniela Buonvicino [a,*], Giuseppe Ranieri [a], Daniele Guasti [b], Alessandra Pistolesi [a], Antonino Iurato La Rocca [c], Elena Rapizzi [d], Alberto Chiarugi [a]

[a] Department of Health Sciences, Section of Clinical Pharmacology and Oncology, University of Florence, Florence, Italy
[b] Imaging Platform, Department of Experimental & Clinical Medicine, University of Florence, Florence, Italy
[c] Department of Neuroscience, Psychology, Drug Sciences, and Child Health (NEUROFARBA),University of Florence, Florence, Italy
[d] Department of Experimental and Clinical Medicine, University of Florence, Florence, Italy

ARTICLE INFO

Keywords:
Progressive EAE
Relapsing-remitting EAE
Mitochondria
Bioenergetics

ABSTRACT

Introduction: Derangement of axonal mitochondrial bioenergetics occurs during progressive multiple sclerosis (PMS). However, whether this is a delayed epiphenomenon or an early causative event of disease progression waits to be understood. Answering this question might further our knowledge of mechanisms underlying neurobiology of PMS and related therapy.

Methods: $MOG_{35–55}$-immunized NOD and $PLP_{139–151}$-immunized SJL female mice were adopted as models of progressive or relapsing-remitting experimental autoimmune encephalomyelitis (EAE), respectively. Multiple parameters of mitochondrial homeostasis were analyzed in the mouse spinal cord during the early asymptomatic stage, also evaluating the effects of scavenging mitochondrial reactive oxygen species with Mito-TEMPO.

Results: Almost identical lumbar spinal cord immune infiltrates consisting of Th1 cells and neutrophils without B and Th17 lymphocytes occurred early upon immunization in both mouse strains. Still, only NOD mice showed axon-restricted dysregulation of mitochondrial homeostasis, with reduced mtDNA contents and increased cristae area. Increased expression of mitochondrial respiratory complex subunits Nd2, Cox1, Atp5d, Sdha also exclusively occurred in lumbar spinal cord of NOD and not SJL mice. Accordingly, in this region genes regulating mitochondrial morphology (Opa1, Mfn1, Mfn2 and Atp5j2) and mitochondriogenesis (Pgc1α, Foxo, Hif-1α and Nrf2) were induced early upon immunization. A reduced extent of mitochondrial derangement occurred in the thoracic spinal cord. Notably, the mitochondrial radical scavenger Mito-TEMPO reduced H_2O_2 content and prevented both mtDNA depletion and cristae remodeling, having no effects on dysregulation of mitochondrial transcriptome.

Discussion: We provide here the first evidence that axonal-restricted derangement of mitochondrial homeostasis already occurs during the asymptomatic state exclusively in a mouse model of PMS. Data further our understanding of mechanisms related to EAE progression, and point to very early axonal mitochondrial dysfunction as central to the neuropathogenesis of MS evolution.

1. Introduction

Several experimental models of multiple sclerosis (MS) have been developed in order to decipher the cellular and molecular mechanisms responsible for disease pathogenesis. Among them, experimental autoimmune encephalomyelitis (EAE) is a reliable model recapitulating some of the immunopathological and neurological features of MS (Palumbo and Pellegrini, 2017). Even though several mouse and rat strains

Abbreviations: ARMD, axonal response of mitochondria to demyelination; CS, citrate synthase; dpi, days post immunization; EAE, experimental autoimmune encephalomyelitis; EDAM, early derangement of axonal mitochondria; MOG, myelin oligodendrocyte glycoprotein; mtDNA, mitochondrial DNA; PEAE, progressive experimental autoimmune encephalomyelitis; PLP, proteolipid protein; PMS, progressive multiple sclerosis; PTX, pertussis toxin; RREAE, relapsing-remitting experimental autoimmune encephalomyelitis; RRMS, relapsing-remitting multiple sclerosis; VDAC1, Voltage-dependent anion-selective channel 1.

* Corresponding author at: Department of Health Sciences, Section of Clinical Pharmacology and Oncology, University of Florence, Viale Pieraccini 6, 50139 Firenze, Italy.

E-mail address: daniela.buonvicino@unifi.it (D. Buonvicino).

https://doi.org/10.1016/j.nbd.2023.106015
Received 21 July 2022; Received in revised form 18 January 2023; Accepted 22 January 2023
Available online 23 January 2023

undergo a pattern of EAE evolution that resembles relapsing-remitting MS (RRMS) (Burrows et al., 2019; Peiris et al., 2007), the feasibility of inducing a pattern of EAE progression that reliably recapitulates immunology, neuropathology, as well as the pattern of neurological impairment found in progressive MS (PMS) patients is still controversial. Inevitably, this difficulty has hampered the understanding of the events responsible for primary or secondary progression. Likewise, lack of a reliable PMS model has undoubtedly delayed the identification of treatments able to counteract neurodegeneration during primary or secondary PMS.

Recently, we reported a detailed neuroimmune characterization of EAE in $MOG_{35–55}$-immunized NOD mice, showing that animals develop a progressive worsening of neurological impairment that invariantly leads *to exitus* within 3–6 months (Buonvicino et al., 2019). Notably, in keeping with PMS patients, EAE progression in NOD mice is insensitive to multiple immunosuppressing agents, in spite of evidence that these drugs do reduce immune-sensitization to MOG in these animals (Buonvicino et al., 2021, 2019). These findings taken together suggest that pathogenesis of EAE in NOD mice recapitulates some features of MS progression (thereby defined as "PEAE"). Further substantiating this assumption, PEAE in NOD mice is featured by a derangement of mitochondrial homeostasis during disease evolution (Buonvicino et al., 2019) similar to that occurring in CNS of PMS patients (Campbell et al., 2014). Given that impairment of mitochondrial bioenergetics is now considered central to neuroaxonal degeneration during PMS, the PEAE NOD mouse model may provide hints useful to decipher whether and how organelle dysfunction participates to pathogenesis of MS progression.

In this regard, several questions related to the role of mitochondrial dysfunction in neurobiology of MS/EAE disease remain unanswered. First, it is still unclear whether organelle dysfunction is a primary trigger of axonal loss or follows derangement of axonal integrity. Second, it waits to be determined whether loss of mitochondrial homeostasis similarly occurs in PMS and RRMS mouse models. Third, it is unknown whether organelle dysfunction exclusively occurs in neurons or is a more general feature of neural cells within the demyelinating regions. Lastly, a clear-cut picture of the functional/structural mitochondrial parameters that are first affected during PEAE development has not been provided.

On this basis, in an attempt to answer these questions, we investigated whether derangement of axonal mitochondrial homeostasis in PEAE NOD mice occurs before symptoms onset (here defined as Early Derangement of Axonal Mitochondria, EDAM). Further, to understand whether findings were specific to the progressive pattern of EAE evolution, EDAM was also investigated in immunized SJL mice, a widely adopted model of RRMS.

2. Materials and methods

2.1. Experimental design

All animal care and experimental procedures were performed according to the European Community guidelines for animal care (European Communities Council Directive 2010/63/EU) and were approved by the Committee for Animal Care and Experimental Use of the University of Florence. Given the well-known 3:1 female:male ratio in MS patients. EAE is typically induced in female animals and indeed only female mice were used in our study. Female NOD/ShiLtj (10 weeks old) and SJL/J (6–8 week old) purchased from Charles River (Milan, Italy) were housed in a conventional unit (5–6 per cage) with free access to food (Harlan Global Diet 2018, Harlan Laboratories, Udine, Italy) and water, and maintained on a 12 h light/dark cycle at 21 °C room temperature.

2.2. EAE induction

EAE was induced in NOD/ShiLtj and SJL/J mice by subcutaneous immunization, with 250 μg of $MOG_{35–55}$ (MEVGWYRSPFSRVVHLYRNGK)and 300 μg of $PLP_{139–151}$ (HSLGKWLGHPDKF) peptide, respectively (both synthesized by EspiKem Srl., University of Florence, Italy), emulsified in complete Freund's adjuvant (CFA) (Sigma, Milan, Italy) containing 4 mg/ml of *Mycobacterium tuberculosis* H37RA (Difco Laboratories, Detroit, MI, USA) in the flanks and at the base of the tail. Immediately thereafter and 48 h later, mice received an intraperitoneal injection (i.p.) of 200 ng **pertussis** toxin (PTX) (Sigma, Milan, Italy) in 100 μl Phosphate-Buffered Saline (PBS) (Buonvicino et al., 2019; Cavone et al., 2015). NOD/ShiLtj- and SJL/J-immunized mice were sacrificed 15 and 7 days after EAE, respectively, when no clinical signs of EAE werereported.NOD/ShiLtj mice were randomized (generating groups by the RAND function of Excel software) and treated with Mito-TEMPO (Sigma, Milan, Italy). Mito-TEMPO were dissolved in PBS and daily administrated i.p. at 1 $mg{\cdot}kg^{-1}$body weight for 15 days from day of immunization.

2.3. Quantitative PCR

Genomic DNA was extracted from mice spinal cord with the Nucleo Spin TriPrep kit (Macherey-Nagel, Duren, Germany). Mitochondrial DNA content was quantified by measuring the ratio between the mitochondrial *Nd1 or Cox1* and nuclear β-*actin* gene amplification products (Felici et al., 2017). The following primers were used: *Cox1* forward 5'-TATCAATGGGAGCAGTGTTTG-3′ and reverse 5'-AGGCCCAGGAAATGTTGAG −3′; *mt-Nd1* forward 5'-TGCCAGCCTGACCCATAGCCATA-3′ and reverse 5'-ATTCTCCTTCTGTCAGGTCGAAGGG-3′; β-*actin* forward 5'-GCAGCCACATTCCCGCGGTGTAG-3′ and reverse 5'-CCGGTTTGGACAAAGACCCAGAGG-3′. Total RNA from mouse spinal cord was isolated using Trizol Reagent (Life Technologies). One μg of RNA was retrotranscribed using iScript (Bio-Rad, Milan, Italy). Real-Time PCR was performed using Rotor-Gene 3000 (Qiagen, Milan, Italy) and the Rotor-Gene TM SYBR® Green PCR Kit (Qiagen, Milan, Italy), the reactions were run at 95 °C for 30 s, 95 °C for 5 s and 60 °C for 15 s for 45 cycles (Buonvicino et al., 2018). The following primers were used: T-bet: forward 5′- TGCCTACCAGAACGCAGAGATCACTC -3′ and reverse 5′- GTAGAAACGGCTGGGAACAGGATACTG −3′; RORγt: forward 5′- CCATTCAGTATGTGGTGGAGTTTGCCAA −3′ and reverse 5′-GCAGCCCAAGGCTCGAAACAGCT -3';LY6G:forward 5′- CAGAAGCAAAGTCAAGAGCAATCTCTGC -3′ and reverse 5′-GTCTGCAGAAGGACTGAAACCAGGCT −3; Opa1:forward 5′-CAGCACAATGCTTTGGAAGACCGGTC -3′ and reverse 5′-CTTGGTTTCGTTGTGAACACACTGCTC -3; Mfn1:forward 5′-CGATTCCTGGGTTCCACAAATGCACAG −3′ and reverse 5′-CGATGATGCCCATGGAGGTTCTCG −3; Mfn2:forward 5′-GTCTATGAGCGACTGACCTGGACCAC-3′ and reverse 5′-CTGCTCCAGATTATCTCGGGTGATGTC-3; Atp5J2:forward 5′-AGAGCTGCCGAGCTGGATAATGATGC -3′ and reverse 5′-GTCGCCGCTCATGTTTGAGTTCCTTG −3; *Pgc1-α*: forward 5′-GACAGATGGAGCCGTGACCACTG-3′ and reverse 5′-CTGATCCTGTGGGTGTGGTTTGC-3; *mt-Nd2* forward 5'-ATTATCCTCCTGGCCATCGTA-3′ and reverse 5'-AAGTCCTATGTGCAGTGGGAT-3′; *Ndufv2* forward 5'-GTGCACAATGGTGCTGGAGGAG-3′ and reverse 5'-GGTAGCCATCCATTCTGCCTTTGG-3′; *Atp5d* forward 5'-CAGCACGGGCTGAGATCCAGAT-3′ and reverse 5'-GACAGGCACCAGGAAGCTTTAAGC-3′; Sdhaforward 5′-CTGCGGCTTTCACTTCTCTGTTGGTG-3′ and reverse 5′-ATCGGGTAGGAAAGAGCTTTGTAAGGC-3; *18S*forward 5'-AAAACCAACCCGGTGAGCTCCCTC-3′ and reverse 5'-CTCAGGCTCCCTCTCCGGAATCG-3′. Primers were purchased from Integrated DNA Technologies (Iowa, USA).

2.4. Immunohistochemistry

For immunohistochemical analysis, lumbosacral spinal cords from control, MOG-immunized NOD or PLP-immunized SJL mice, were

collected; 10-μm thin sections were blocked with 5% normal goat serum (Thermo Fisher Scientific, Waltham, MA, USA) containing 0.3% Triton X-100 (Sigma, Milan, Italy). One hour later, sections were incubated overnight at 4 °C with a CD4 monoclonal antibody (1:200, Cat# 4SM95, ThermoFisher) or with LY6G monoclonal antibody for neutrophils (1:200, Cat# ab25377, Abcam). After washings, sections were incubated with an anti-rat secondary antibody conjugated with AlexaFluor 546 (1:2000, Cat# A-11035, Thermo Fisher Scientific). Images were acquired under a LEICA TCS SP5 confocal laser scanning microscope (Leica Microsystems CMS GmbH, Mannheim, Germany) with a 20× objective (Buonvicino et al., 2020).

2.5. Transmission electron microscopy

Transmission electron microscopy was performed as previously described (Felici et al., 2017). Briefly, the spinal cord was fixed in Karnovsky's solution, post-fixed in 1% osmium tetroxide and embedded in Epon 812. Ultrathin sections were stained with uranyl acetate and alkaline bismuth subnitrate and examined under a JEM 1010 electron microscope (Jeol, Tokyo, Japan) at 80 kV. Micrographs were taken at final magnifications of 25,000× and 80,000× using a Mega View III digital camera and interfacing software (SIS-Soft Imaging System, Munster, Germany). To analyze the cristae area, only mitochondria unequivocally present within axoplasmic fields were analyzed. Areas of cristae were measured using iTEM image analysis software (SIS).

2.6. Western blotting

Lumbar spinal cord tissue was dissolved in 1% SDS. BCA (bicinchoninic acid) Protein Assay was used to quantify the total protein levels. Lysates (20 μg/lane of protein) were resolved by electrophoresis on a 4–20% SDS-polyacrylamide gel (Bio-Rad Laboratories, Hercules, CA, USA) and transferred onto nitrocellulose membranes. After blocking, the blots were incubated overnight at 4 °C with anti-VDAC1 (Cat# ab14734, Abcam, Cambridge, London, UK), anti-SDHA (Cat# ab14715, Abcam, Cambridge, London, UK), anti-Cytochrome c oxidase (OxPhos Complex IV) (Cat# A21348, Thermo Fischer Scientific), anti-PGC1α (Cat# A12348, ABclonal, Woburn, United States), anti-ND2 (Cat# A6180, ABclonal, Woburn, United States), anti-ATP5D (Cat# A9929, ABclonal, Woburn, United States), anti-FOXO1 (Cat# A17978, ABclonal, Woburn, United States), in TBS-T containing 5% bovine serum albumin. Anti-Tubulin (T9026, monoclonal antibody, Sigma, St. Louis, MO, USA), anti-β-Actin (A1978 monoclonal antibody, Sigma, St. Louis, MO, USA) or anti-GAPDH (G8795 monoclonal antibody, Sigma, St. Louis, MO, USA) were used as a loading control. Immunodetection was performed with HRP-conjugated secondary antibodies (diluted 1:2000 anti-mouse) (Amersham Biosciences, Little Chalfont, UK) in TBS-T containing 5% non-fat dry milk. After washing, the membranes were detected using chemiluminescence (ECL plus; Euroclone, Padova, Italy). Quantity One analysis software was used for quantitative analysis (Bio-Rad, Hercules, CA, USA). Results are presented as the mean standard error of the mean (SEM) of different gels and expressed as AU-, which depicts the ratio between levels of target protein expression and tubulin or GAPDH normalized to basal levels (Landucci et al., 2021).

2.7. Citrate synthase (CS) activity

Homogenates were prepared as already described (Rapizzi et al., 2012) with minor modifications. Briefly, dissected lumbar spinal cord tissue was chopped finely, resuspended in a solution containing 120 mM KCl, 20 mM HEPES, 2 mM $MgCl_2$, 1 mM EGTA, 5 mg/ml BSA, and homogenized in a hand held homogenizer. The homogenate was centrifuged at 800*g* for 10 min at 4 °C and supernatants were quantified for protein content (Coomassie Blue reagent was from Bio-Rad, Hercules, CA, USA). All procedures were carried out on ice, or at 4 °C.

CS activity was measured incubating the tissue homogenate supernatants (25 μg/sample, in duplicates) in a Tris buffer containing acetyl-coenzyme A, 5,5'dithiobis(2-nitrobenzoic acid), and oxaloacetate, and measuring the increase in absorbance at 412 nm (Rapizzi et al., 2012). The enzymatic activities were evaluated by photometry using the Victor3 1420 Multilabel Counter (Packard Instruments, Perkin-Elmer).

2.8. H_2O_2 assay

H_2O_2 levels were assessed in spinal cord tissue by using the Amplex Red® assay (Invitrogen). Briefly, tissue was rapidly removed and placed into modified Krebs/HEPES buffer (composition in mmol/l: 99.01 NaCl, 4.69 KCl, 2.50 $CaCl_2$, 1.20 $MgSO_4$, 1.03 KH_2PO_4, 25.0 $NaHCO_3$, 20.0 Na-HEPES, and 5.6 glucose [pH 7.4]). Samples were minced and incubated with Amplex red (100 μM) and HRP (1 U/ml) (1 h, 37 °C) in modified Krebs/HEPES buffer protected from light. Fluorescence excitation and emission were at 540 and 590 nm, respectively. H_2O_2 production was calculated using H_2O_2 standard and expressed as mmol/l of mg of dry tissue (De Logu et al., 2021).

2.9. Statistical analysis

Data are expressed as mean ± SEM. All differences among groups were performed using Student's *t*-test or ANOVA followed by Tukey's W-test. Levels of significance were $p < 0.05$ (*), $p < 0.01$ (**), and $p < 0.001$ (***). Statistical analyses were carried out using Graph Pad Prism (version 7).

3. Results

3.1. Evaluation of immune infiltrates in the lumbosacral spinal cord of immunized NOD and SJL mice before disease onset

As shown in Fig. 1A, and in keeping with prior work (Buonvicino et al., 2019; Cavone et al., 2015), disease onset in NOD and SJL mice occurred 30 ± 7and 13 ± 4 days post immunization (dpi), respectively. We therefore first checked whether immune infiltrates were already present in the mouse lumbar spinal cord at time points anticipating the appearance of neurological impairment. We selected 15 and 7 dpi for NOD ad SJL mice, respectively, corresponding to the half of the asymptomatic phase for each strain (Fig. 1A). Given that these time points represent early asymptomatic stages of EAE development, immune infiltrates were evaluated by means of RT-PCR to increase the sensitivity of the analysis. As shown in Fig. 1B, in asymptomatic NOD mice Th1 and neutrophil infiltrates increased 3- and 4-fold, respectively, whereas neither B nor Th17 lymphocytes showed a significant change compared to non-immunized animals. Of note, an almost identical pattern of immune cell infiltration was found in asymptomatic 7 dpi SJL mice (Fig. 1C). In order to confirm PCR data and reveal a possible different localization of Th1 or neutrophil infiltrates, in the two different strains we also evaluated these two cell populations by means of immunohistochemistry. We found that, albeit very rare, CD4+ cells were similarly distributed in the mouse spinal cord of both strains (Fig. 1D), whereas LY6G+ neutrophils were undetectable in these animals (data not shown). Possibly, the scant neutrophil infiltrates at the early asymptomatic stage could explain the apparent discrepancy between RT-PCR and immunohistochemistry results. Even though the quantitative aspects of both spinal cord infiltrates were consistent with the early stage of EAE, the similarity between the two mouse strains was somehow surprising in light of their different type of EAE evolution (Fig. 1A).

3.2. EDAM in the lumbar spinal cord of NOD and SJL mice

Prior work showed a progressive reduction of both mtDNA and cristae area of axonal mitochondria in the spinal cord of PEAE NOD mice during disease evolution (Buonvicino et al., 2019). To better understand

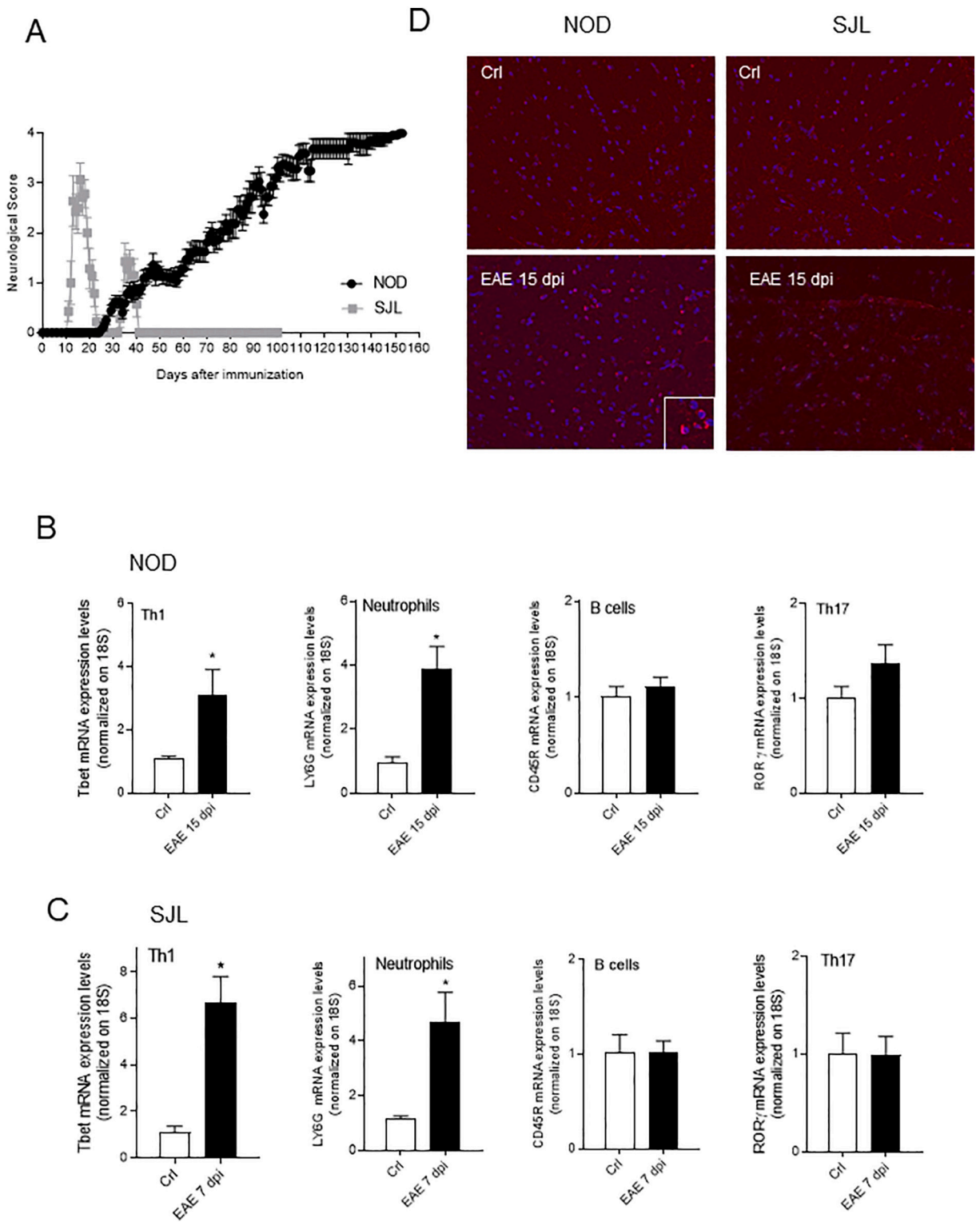

Fig. 1. EAE evolution and lumbar spinal cord inflammatory infiltrates in NOD and SJL mice after EAE induction. (A) Evolution of neurological disability in NOD mice immunized with MOG_{35-5} and SJL mice immunized with $PLP_{139-151}$. Th1 (T bet$^+$), neutrophil (LY6G+), B (CD45R+) and Th17 (RORyt$^+$) infiltrates in the lumbar spinal cord ofMOG-immunized NOD mice at day 15 post-immunization (B) or PLP-immunized SJL mice at day 7 post-immunization (C) compared to controls. (D) Representative confocal images (20×) of CD4+ cells in the spinal cord of 15 dpi NOD mice and 7 dpi SJL animals. In (A) each point is the mean ± SEM of at least 25 mice per group. In (B and C) each column is the mean ± SEM of at least 5 mice per group.*$p < 0.05$ vs Crl (Student's *t*-test).

onset and strain-specificity of mitochondrial homeostasis derangement, we first evaluated the number of axonal mitochondria within the lateral columns of the lumbar spinal cord in asymptomatic NOD and SJL mice. We found that the number of axonal mitochondria did not change in 15 dpi NOD and 7 dpi SJL mice compared to controls (Fig. 2A and B). Consistently, expression levels of voltage-dependent anion channel (VDAC), a highly represented protein of the external mitochondrial membrane and prototypical marker of organelle content (Lee et al.,

2019), did not differ between the two strains as well as upon immunization (Fig. 2C and D). However, when levels of mtDNA (evaluated by quantifying contents of mitochondrial genes Nd1 and Cox1 compared to nuclear β-actin) were analyzed, we found that they were reduced in the lumbar spinal cord of 15 dpi NOD mice (Fig. 2E), showing no change in 7 dpi SJL animals (Fig. 2F). Importantly, these findings, on the one hand, indicated that mitochondrial homeostasis is indeed affected before onset of EAE, thereby substantiating the occurrence of EDAM, but on the other also disclosed that EDAM appeared an exclusive feature of NOD mice, the strain prone to disease progression.

To gather additional information on this important pathogenetic hint, we next evaluated additional parameters of mitochondrial homeostasis. It is well known that the bioenergetic status of the organelle can prominently affect its structure (Kondadi et al., 2019; Perkins and Ellisman, 2011). In the lumbar spinal cord of asymptomatic NOD and SJL mice, we therefore evaluated size and morphology of axonal mitochondria. In keeping with data on mitochondrial number, we found that even mitochondrial areas did not change in lumbar spinal cord axons of both mouse strains (Fig. 3A and B). However, the area of cristae significantly increased in axonal mitochondria of immunized NOD mice compared to controls, showing, again, no changes in SJL mice (Fig. 3C). This NOD-specific change of mitochondrial structure is in keeping with data on mtDNA content (see Fig. 2E and F). It is well known that several genes including Opa1, Mnf1, Mnf2 and Atp5j2 regulate morphology and structural rearrangements of mitochondria (Alavi and Fuhrmann, 2013; Galber et al., 2021; Kondadi et al., 2020). We, therefore, analyzed their transcriptional levels in the lumbosacral spinal cord of immunized NOD mice and found that they were indeed significantly increased compared to control mice (Fig. 3D).

Next, given that NOD mice at the advanced stage of PEAE show reduced expression of several nuclear- and mitochondria-encoded respiratory complex subunits (Buonvicino et al., 2019), a feature also described in a chronic model of EAE (Schattling et al., 2019), we also evaluated whether transcriptome of respiratory complex subunits is already altered in the asymptomatic stage. Strikingly, instead of a decrease we found a substantial increase in transcription of all the respiratory complex subunits analyzed in the lumbar spinal cord of NOD mice, whereas no changes occurred in SJL mice (Fig. 4A and B). In keeping with transcriptomic analysis, protein levels of mitochondrial complex I ND2 subunit, complex II SDHA subunit, complex IV cytochrome *c* oxidase COX1 subunit, and complex V ATP5D subunit also increased in the lumbar spinal cord of NOD mice (Fig. 4C and D).

To gather additional information on EDAM, we also evaluated the spinal cord activity of mitochondrial citrate synthase, the first enzyme of the Krebs's cycle. Consistent with our findings indicating a selective activation of mitochondrial metabolism exclusively in mice prone to EAE progression, citrate synthase activity increased upon immunization in the lumbar spinal cord of NOD but not SJL animals (Fig. 5A and B).

Finally, the substantial changes of mitochondrial morphological and bioenergetic parameters in lumbar spinal cord of NOD mice prompted us to evaluate whether concomitant changes occurred at the level of key nuclear transcription factors involved in the regulation of organelle homeostasis such as Pgc1α, Foxo1, Nrf2 and Hif-1α. Of note, we found that their transcripts were significantly increased at this early EAE stage in the lumbar spinal cord, with the exception of Hif-1α which only showed a tendency to increase (Fig. 5C). However, protein levels of PGC1α and FOXO1, did not increase in the lumbar spinal cord of these animals (Fig. 5D and E). Collectively, data indicate that EDAM occurs during the asymptomatic stage of EAE, but appears an exclusive feature of the progressive and not of the relapsing-remitting pattern of the disease.

3.3. Immune infiltrates and EDAM in the thoracic spinal cord of NOD mice

It is well acknowledged that neuroinflammatory infiltrates accumulate in rodents with EAE, including NOD mice, following a time-dependent, caudo-cranial gradient (Kummari et al., 2019; Pöllinger et al., 2009). We therefore asked whether EDAM was also present in the thoracic spinal cord of NOD mice. Somehow unexpectedly, we found that immune infiltrates were identical to those present in the lumbar tract (Fig. 6A, compare with 1B). However, the parameters of EDAM were less pronounced in upper than in the lower spinal cord region. Specifically, the Nd1 mtDNA gene copy number was reduced in the thoracic spinal cord of immunized NOD mice, whereas the Cox1 gene reduction did not reach statistical significance (Fig. 6B). Accordingly, neither areas of mitochondria nor that of their cristae were altered in the thoracic region of immunized mice compared to controls (Fig. 6C and D). Further suggesting a reduced degreed of EDAM in this spinal cord tract, only two out of five transcripts of respiratory complex subunits were increased in the thoracic spinal cord of asymptomatic NOD mice (Fig. 6E).

3.4. Extra-axonal and hepatic EDAM in immunized NOD mice

We next wondered whether EDAM exclusively occurs in axons destined to degenerate at delayed phases of EAE progression or is part of a more general response to immunization in NOD mice, thereby also occurring in extra-axonal spinal cord structures and/or peripheral organs. Cristae rearrangement was therefore evaluated in mitochondria located outside spinal cord axons, as well as the liver of asymptomatic NOD mice. Remarkably, the cristae area did not change in extra-axonal spinal cord mitochondria (Fig. 7A). In keeping with this, copy numbers of mtDNAgenesNd1 and Cox1 (Fig. 7B), as well as mitochondrial respiratory complex subunit mRNAs (Fig. 7C) were not affected in the liver of NOD mice upon immunization.

3.5. Effects of Mito-TEMPO on multiple spinal cord parameters in immunized NOD mice before disease onset

Several lines of evidence indicate that derangement of the mitochondrial respiratory chain is a key event in oxygen radical formation and neurodegeneration (Picca et al., 2020; Wang et al., 2019). This notion, along with evidence of EDAM found in the spinal cord axons of NOD, prompted us to investigate whether changes of mitochondrial homeostasis were, at least in part, due to ROS production within organelles. To this end, we treated NOD mice with Mito-TEMPO, a mitochondria-targeted superoxide dismutase mimetic with superoxide and alkyl radical scavenging properties (Dikalova et al., 2010; Liang et al., 2010), also active in vivo (Liu et al., 2018; Shetty et al., 2021). We first checked whether systemic treatment with Mito-TEMPO (1 mg/kg, i.p.) affects the neuroimmune response during the asymptomatic stage (15 dpi). Fig. 8A shows that the scavenger did not alter Th1, Th17 and neutrophil infiltrates at this early time point of disease development. We next evaluated hydrogen peroxide contents (a prototypical index of ROS formation) in the lumbar spinal cord of NOD mice. Interestingly, although we found that they tended to increase in immunized mice without reaching statistical significance, daily administration of Mito-TEMPO significantly reduced their spinal cord content (Fig. 8B). Remarkably, reduction of spinal cord hydrogen peroxide contents by the mitochondrial radical scavenger sufficed to prevent mtDNA loss (Fig. 8C), and also counteracted the increase of mitochondria cristae area (Fig, 8D). In spite of these effects, however, treatment with Mito-TEMPO was unable to affect transcript levels of genes Pgc1α, Foxo1, Nrf2 and Hif-1α coding for proteins regulating mitochondrial homeostasis (Fig. 8E), as well as those coding for mitochondrial respiratory complex subunits Nd2, Cox1, Ndufv2, Atp5d and Sdha (Fig. 8F) that we found increased in the lumbosacral spinal cord of NOD mice upon immunization.

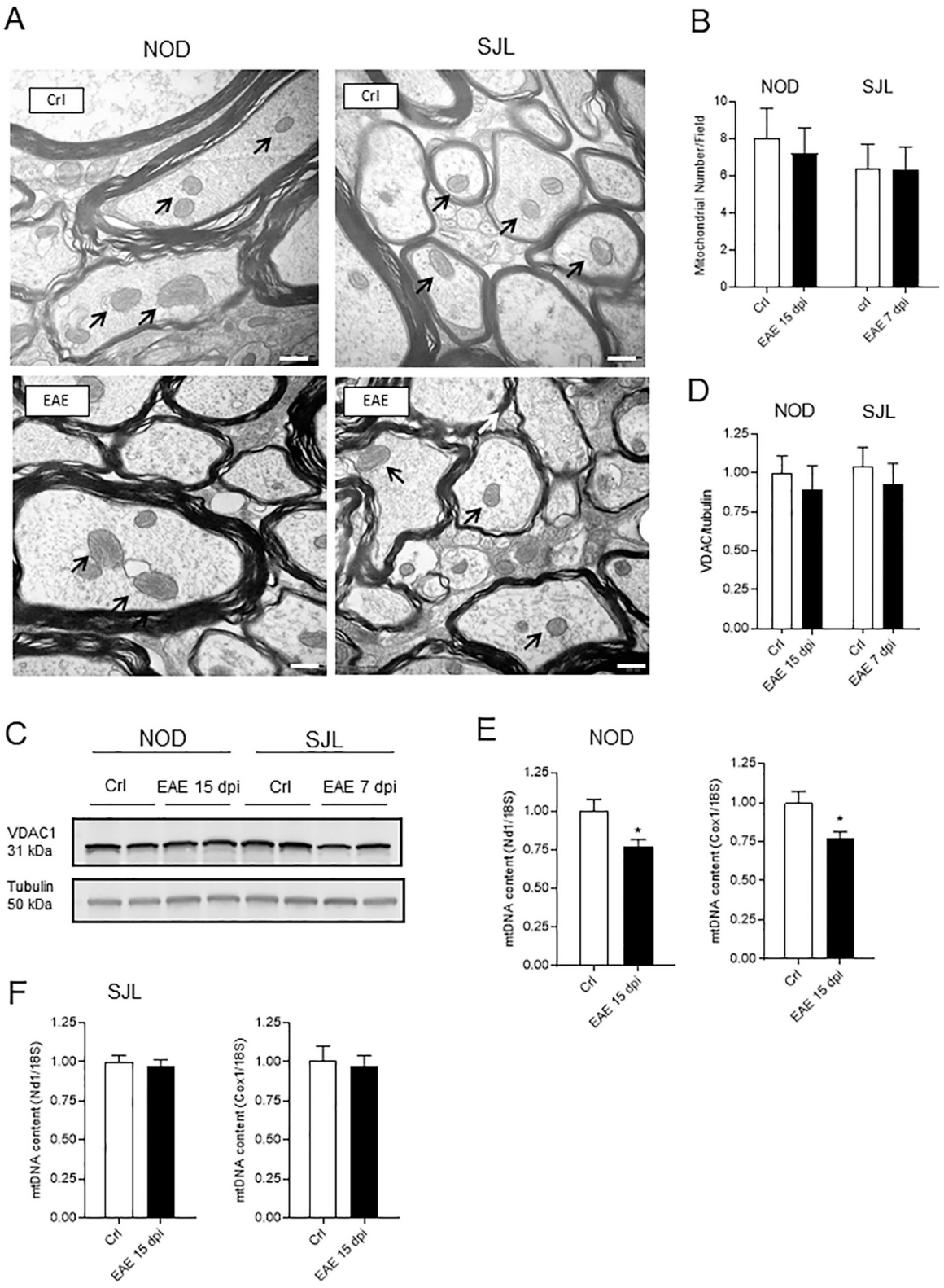

Fig. 2. Characterization of mitochondrial number and mtDNA content in the lumbar spinal cord of NOD and SJL mice after EAE induction. Representative EM images (25.000×) (A) and quantitation (B) of mitochondrial number within axons of spinal cord lateral columns in NOD and SJL mice at day 15 and 7 post-immunization compared to controls, respectively. Black arrows indicate axonal mitochondria. Representative (C) and densitometric analysis (D) of VDAC1 expression levels in the lumbar spinal cord of control or NOD and SJL mice at days 15 and 7 post-immunization, respectively. mtDNA content in the lumbar spinal cord of NOD (E) and SJL (F) mice compared to controls at day 15 and 7 post-immunization, respectively. In (A) scale bar is 2 μm. In (B) each column is the mean ± SEM of 5 mice per group. In (D) each column is the mean ± SEM of at least 7 mice per group. In (E and F) each column is the mean ± SEM of at least 8 animals per group. *$p < 0.05$ vs Crl (Student's t-test).

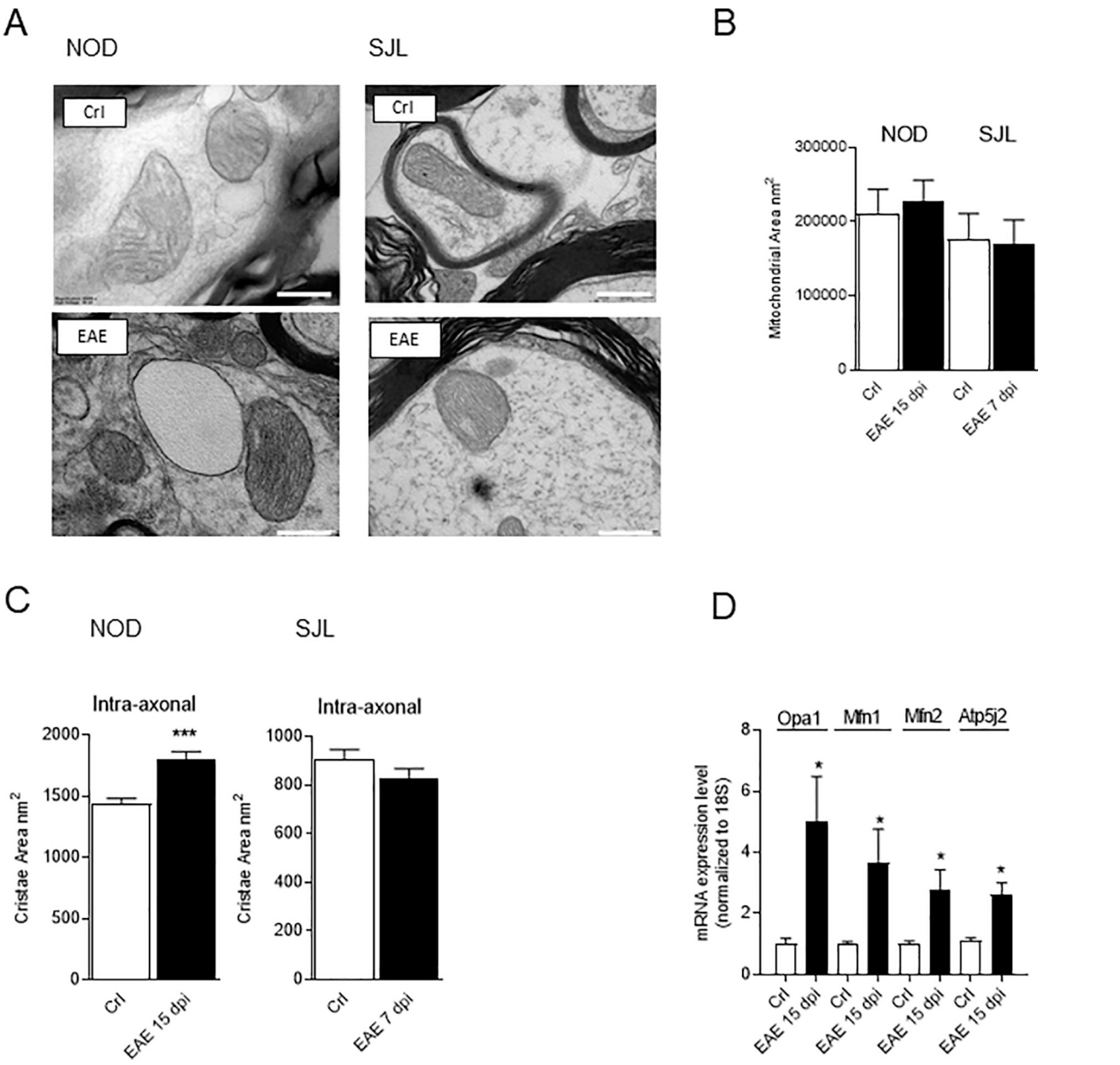

Fig. 3. Characterization of mitochondrial area and cristae in the lumbar spinal cord of NOD and SJL mice after EAE induction. (A) Representative EM image (magnifications 50.000×) showing the morphology of cristae of axonal mitochondria within the lumbar spinal cord lateral columns in control or NOD and SJL at day 15 and 7 post-immunization, respectively. (B) Area of mitochondria within axons of lumbar spinal cord lateral columns as in (A). (C) Cristae area of mitochondria within axons of spinal cord lateral columns in control or NOD and SJL mice at day 15 and 7 post-immunization, respectively. (D) mRNA levels of mitochondrial genes Opa1, Mnf1, Mnf2 and Atp5j2 in the spinal cord of control or NOD mice at day 15 post-immunization. In (A) scale bar is 200 nm. In (B, C and D) each column is the mean ± SEM of at least 5 mice per group. In (C) about 800 mitochondrial cristae areas belonging to control or immunized mice were measured. *$p < 0.05$ vs Crl (Student's t-test).

4. Discussion

We report here that axonal mitochondrial homeostasis is perturbed well before symptom onset in a model of PEAE, being however unaffected in a model of RREAE. To our knowledge, this is the first evidence of a selective link between EDAM and progressive evolution of EAE. At present, we do not know the molecular machinery involved in sensing perturbation of immune homeostasis within the spinal cord, and triggering EDAM selectively within axons. In principle, EDAM can be interpreted as a sort of homeostatic response aimed at increasing mitochondrial functioning, even though, at that very early moment of PEAE evolution, reasons requiring bioenergetic boosting within spinal cord axons are not easy to be identified. Regardless, evidence that EDAM exclusively occurs in an EAE model characterized by widespread axonal loss (Buonvicino et al., 2020, 2019) points to a link between EDAM, neurodegeneration and disease progression. It is also worth noting that our finding showing that SJL mice present a pattern of spinal cord immune infiltrates quantitatively and qualitatively identical to that of NOD mice indicates that the neuroimmune response is not, per se, responsible for EDAM. Possibly, EDAM stems from axonal sensing of the first wave of immune infiltrates in a mouse strain with a genetic background that predisposes to neurodegeneration upon immunization. In this light, we hypothesize that the progression of EAE in NOD mice may be due to their ability to prompt EDAM that, in a condition of chronic immune invasion, turns into a key trigger of progressive axonopathy. Prior work indicates that Treg of NOD mice are dysfunctional, a trait that has been

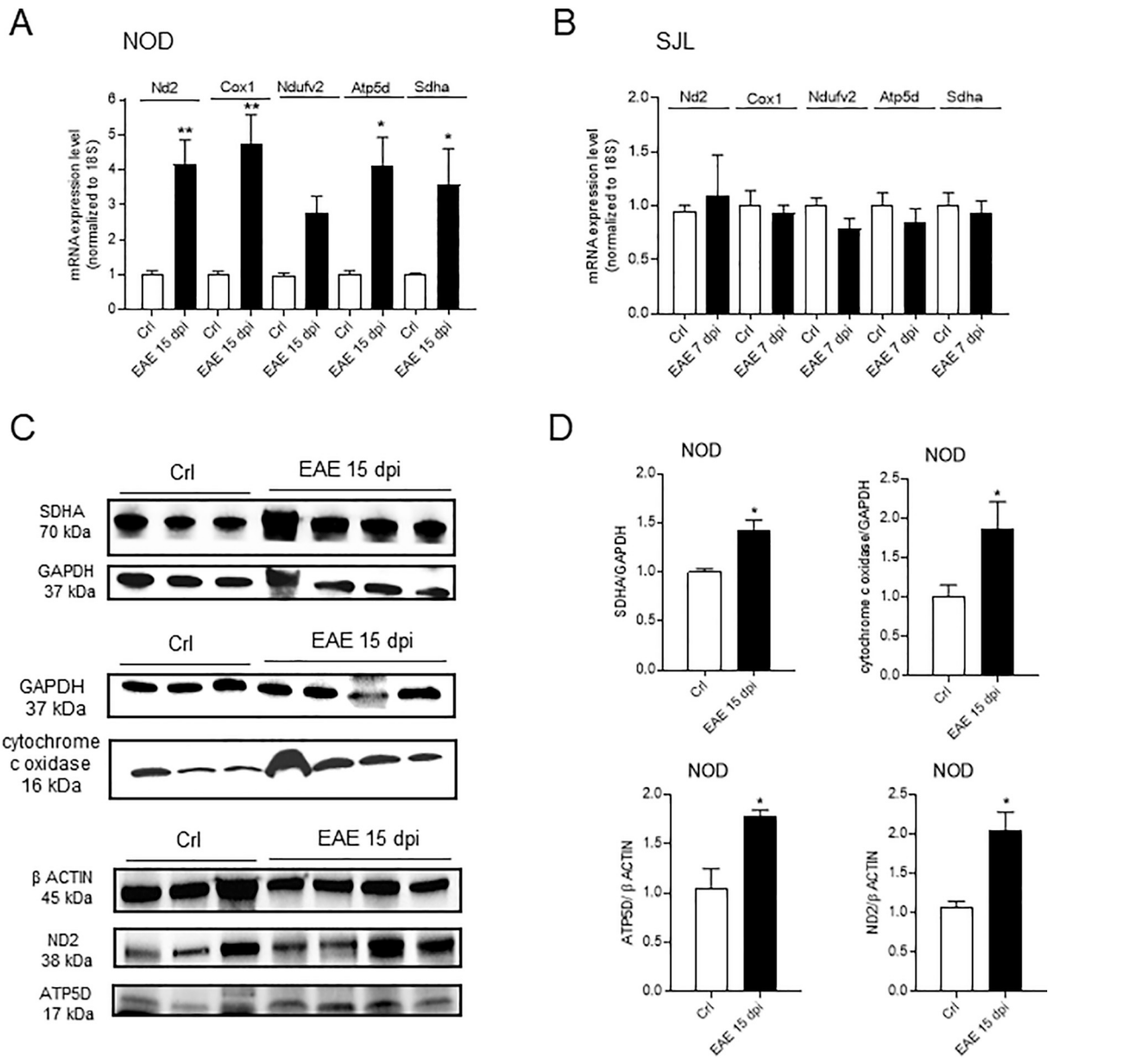

Fig. 4. Respiratory complex subunits in the lumbar spinal cord of immunized NOD and SJL mice. mRNA levels of nuclear (Ndufv2, Atp5d and Sdha) and mitochondrial (Cox1, and Nd2) respiratory complex subunits in the spinal cord of control or NOD (A) and SJL (B) mice at day 15 and 7 post-immunization, respectively. Expression levels (C) and densitometric analysis (D) of SDHA, Cytochrome c oxidase, ND2 and ATP5D in the lumbar spinal cord of control or 15 dpi NOD mice. In (A, B and D) each column is the mean ± SEM of at least 5 mice per group. *p < 0.05, **$p < 0.01$ vs Crl (Student's t-test).

hypothesized to predispose to unrestrained autoimmune responses (D'Alise et al., 2008; James et al., 2016), possibly also including those underlying PEAE. We reason, however, that even though this might well participate to the late events that follow disease onset and sustain progression, it would unlikely be responsible for EDAM. Indeed, the identical immune infiltrates in NOD and SJL mice during the early asymptomatic state, suggest that at this time point Treg dysfunction of NOD animals is not yet functionally relevant and responsible for EDAM. This assumption is corroborated by evidence that Th17 lymphocyte infiltrates are absent in both NOD and SJL mice at 15 dpi, a finding at odds with the possibility that Treg dysfunction in NOD mice potentiates the autoimmune response and, in turn, prompts EDAM.

In a previous study, we reported mtDNA reduction in PEAE NOD mice at score 1 and more pronounced reductions at later stages of disease evolution (Buonvicino et al., 2019). In that study, we considered mtDNA content reduction as an index of axonal loss but, in light of present data, we need to reconsider our assumption. Indeed, we now show that mtDNA reduction is already present in the spinal cord of NOD mice at 15 dpi, a time points with no evidence of axonal mitochondria reduction in number or swelling, axonopathy as well as neurological impairment. Further, the extent of mtDNA loss we found in score 1 NOD mice (Buonvicino et al., 2019) is almost identical to that we now report at 15 dpi (Fig. 2E). Overall, data suggest the existence of neuronal sensing of spinal cord perturbations at the beginning of neuroimmune infiltration, and activation of signaling that primarily impinge upon axonal mitochondrial homeostasis.

Evidence of mtDNA reduction appears at odds with that showing maintenance of organelle number and area in the spinal cord of NOD mice (Fig. 2A-D). We reason that during EDAM only some parameters of mitochondrial homeostasis are altered, with organelle swelling being an index of delayed dysfunction of membrane permeability and matrix ion homeostasis. Importantly, however, mtDNA reduction concomitant to

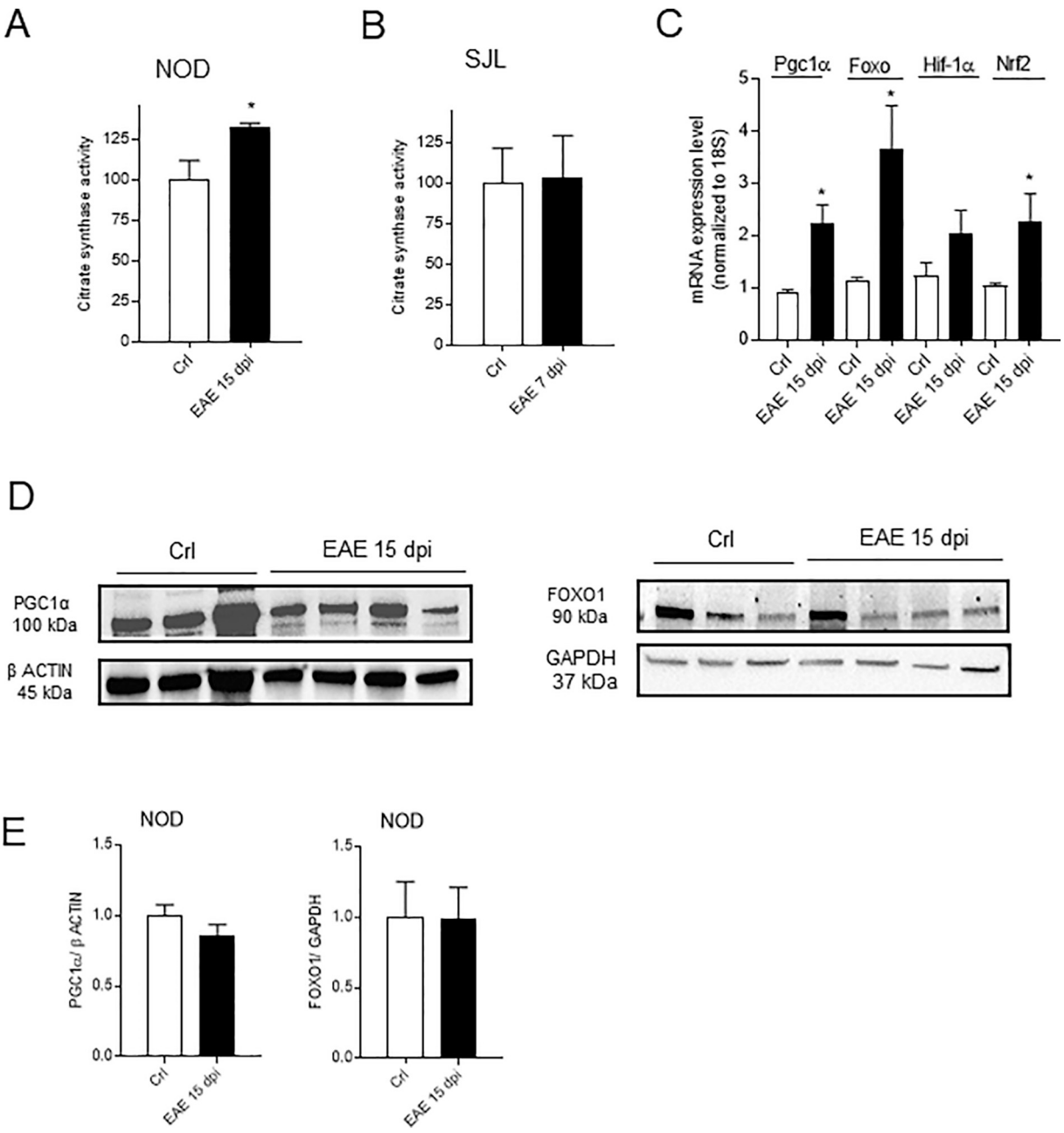

Fig. 5. Citrate synthase activity and genes involved in mitochondriogenesis in the lumbar spinal cord of immunized NOD and SJL mice. Citrate synthase activity in the spinal cord of control or NOD (A) and SJL (B) at day 15 and 7 post-immunization, respectively. (C) mRNA expression levels of Pgc1α, Foxo1, Nrf2 and Hif-1α in the spinal cord of control or NOD mice at day 15 post-immunization. Expression levels (D) and densitometric analysis (E) of PGC1α and FOXO1 in the lumbar spinal cord of control or 15 dpi NOD mice. In (A-C and E) each column is the mean ± SEM of at least 5 mice per group. *$p < 0.05$, **$p < 0.01$ vs Crl (Student's t-test).

unaffected mitochondrial number can be explained considering the change of mitochondrial cristae morphology. It is known, indeed, that mtDNA is strictly bound to cristae and that the complex molecular apparatus that shapes their morphology also regulates mtDNA replication (Kondadi et al., 2020, 2019). Hence, the rearrangement of cristae architecture may explain the loss of mtDNA concomitant to the maintenance of mitochondrial number. A key finding of the present study is evidence that master regulators of mitochondrial biogenesis and shaping such as Pgc1α, Foxo, Nrf2, Hif1α, Opa1, Mfn-1, Mfn-2 and Atp5j2a are all induced during the asymptomatic stage in the spinal cord of NOD mice. This is in keeping with axonal cristae rearrangements and indicates that complex signaling impinging upon mitochondrial transcriptome homeostasis is triggered early after immunization. In keeping with this, several respiratory complex subunits also undergo induction at this early disease stage. In this regard, a very recent study demonstrates that loss of Pgc1α activity in C57Bl mice with EAE correlates with reduced expression of respiratory complex subunits while boosting Pgc1α activity improves neuronal respiratory capacity and EAE clinical score (Rosenkranz et al., 2021). However, our data report a more complex scenario, indeed the unchanged protein levels of PGC1α with concomitant respiratory complex subunits increase, suggesting that several transcriptional regulators could contribute to mitochondrial biogenesis. Of note, in spite of transcript Pgc1α induction, we found concomitant reduction of mtDNA. This is in keeping with prior work showing lack of direct relationship between mtDNA content and mitochondrial biogenesis (Sogl et al., 2000). Further, how, in addition to Pgc1α, several factors such as ATP and nucleotide availability as well as replication origin regulation control mtDNA is still unclear (Filograna

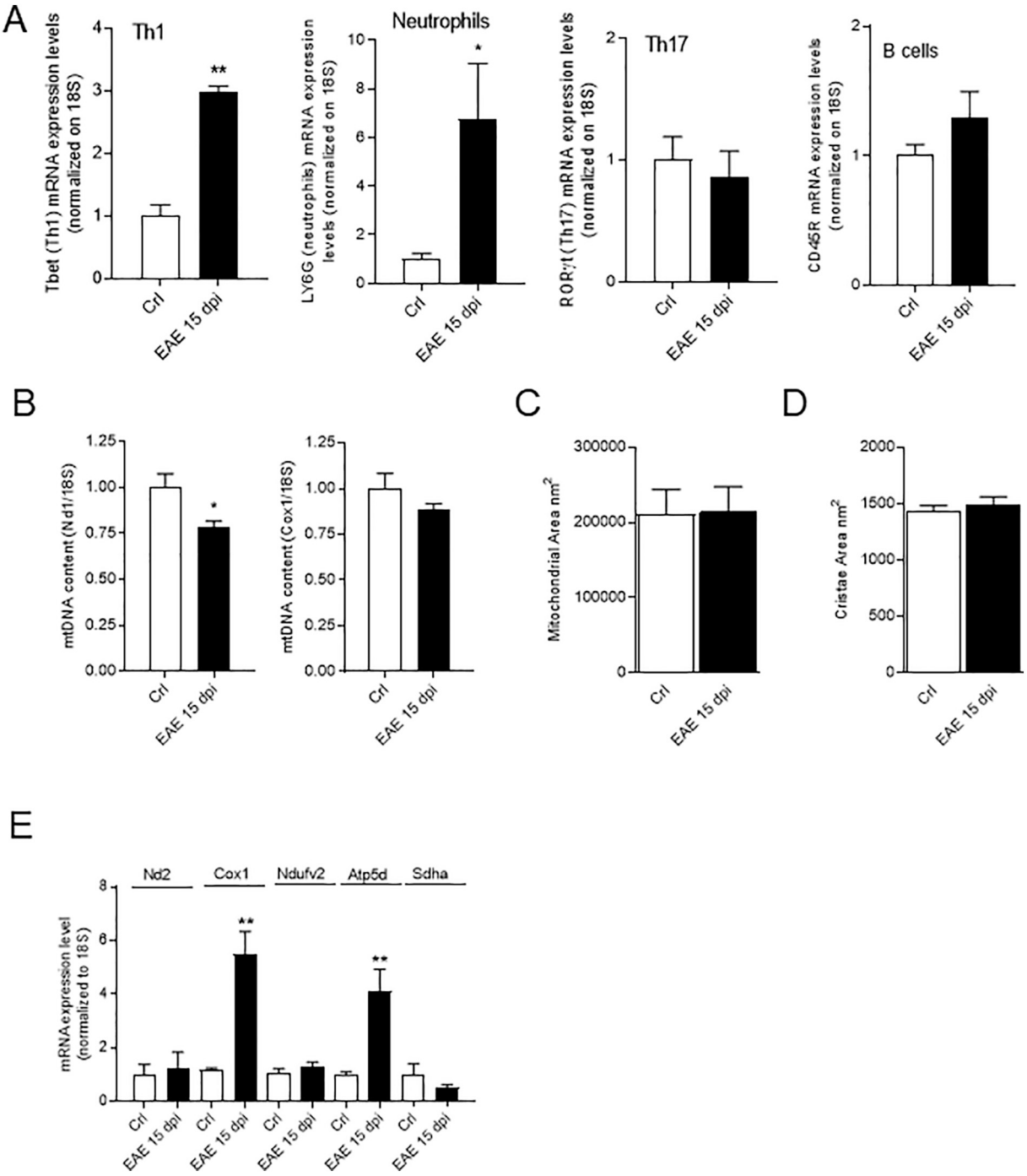

Fig. 6. Mitochondrial parameters in the thoracic spinal cord of NOD mice after EAE induction. (A) Gene expression levels of T bet+-Th1, LY6G- neutrophil, CD45R- B cells and RORyt+-Th17 cells in the thoracic spinal cord of control or MOG-immunized NOD mice at day 15 post-immunization. (B) mtDNA content in the thoracic spinal cord of control or NOD mice at day 15 post-immunization. Mitochondrial area (C) and mitochondrial cristae area (D) within axons of thoracic spinal cord lateral columns in control or NOD mice at day 15 post-immunization. (E) mRNA levels of nuclear (Ndufv2, Atp5d and Sdha) and mitochondrial (Cox1, and Nd2) respiratory complex subunits in the thoracic spinal cord of control or NOD mice at day 15 post-immunization. In (A-E) each column is the mean ± SEM at least of 5 mice per group. In (D) about 600 mitochondrial cristae areas belonging to control or immunized mice were measured. *$p < 0.05$, **$p < 0.01$ vs Crl (Student's t-test).

et al., 2021; Moraes, 2001).

Remarkably, we found no evidence of cristae remodeling in extra-axonal mitochondria, indicating that this event and underling signaling is strictly neuronal. We reason, therefore, that even those parameters for which a neuronal localization is not possible such as mtDNA reduction, transcriptome changes, as well as increase of citrate synthase activity may be axon specific. If that would be the case, given that we normalize PCR data to ribosomal 18S transcripts, then the quantitative aspects of the different parameters of EDAM would be even more pronounced. We would also like to point out that evidence that SJL mice do not undergo neither EDAM nor axonopathy further suggests that EDAM found in NOD mice is exclusively axonal.

As mentioned above, signaling involved in neuronal sensing of early immune infiltrates waits to be identified. In this regard, several lines of evidence indicate a spatially- and timely-regulated response of axonal mitochondria to demyelination. In particular, migration of neuronal

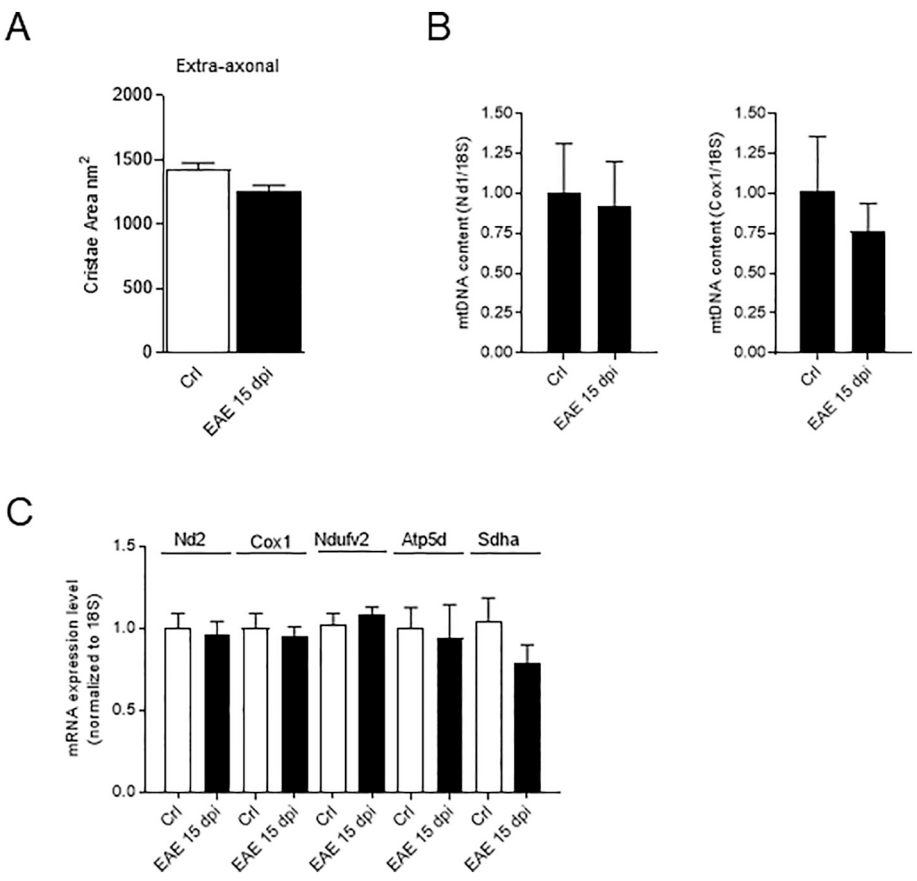

Fig. 7. Mitochondrial parameters in extra-axonal regions of the lumbar spinal cord and liver of NOD mice after EAE induction. (A) Cristae area of extra-axonal mitochondria within the spinal cord lateral columns in control or NOD mice at day 15 post-immunization. (B) mtDNA content in the liver of control or NOD mice at day 15 post-immunization. (C) mRNA levels of nuclear (Atp5d and Ndufv2) and mitochondrial (Cox1, and Nd2) respiratory complex subunits in the liver of control or NOD mice at day 15 post-immunization. In (A-C) each column is the mean ± SEM of at least 5 mice per group. *$p < 0.05$, **$p < 0.01$ vs Crl (Student's t-test).

mitochondria from somata to sites of myelin loss (the so-called "axonal response of mitochondria to demyelination", ARMD) occurs both in animals (Andrews et al., 2006; Diaz et al., 2005) and MS patients (Campbell and Mahad, 2018). This unequivocally suggests a molecular machinery within axon capable of signaling increased energy requirement to somata. Whether this feedback response, in addition to the ability of triggering organelle migration, also includes activation of transcriptional programs regulating mitochondrial homeostasis similar to those of the EDAM waits to be demonstrated. However, lack of evidence of axonal demyelination in asymptomatic 15 dpi NOD mice suggests that ARMD may hardly underpin EDAM. We also would like to point out that while it makes sense for neurons sending mitochondria to sites of axonal energy derangement, the finalistic nature of EDAM appears less clear. Again, the possibility exists that, at variance to ARMD, EDAM is not neuroprotective and merely represents an abnormal response to neuroinflammation contributing to disease progression. However, evidence that genes promoting mitochondriogenesis occurs during EDAM, together with data showing that Pgc1α sustains bioenergetics and protects form EAE (Rosenkranz et al., 2021), corroborate the hypothesis that EDAM represents a protective axonal response early during neuroinflammation, destined to abort at later time points. Why this apparently beneficial event exclusively occurs in a model of EAE-induced axonopathy remains to be understood. Still, it would be highly informative to understand whether PPMS patients are predisposed to EDAM, and the latter is activated when the RRMS turns into SPMS. Interestingly, a very recent contribution shows derangement of mitochondrial bioenergetics in neuronally-enriched extracellular vesicles from plasma of MS patients and that it correlates with severity of brain atrophy (Ladakis et al., 2022). This important finding suggests that analogous analysis can be performed to obtain proof of EDAM in the very early stages of disease evolution of PMS patients.

Because of the well-known ability of mitochondrial respiration to function as a key source of reactive oxygen radicals (ROS), and the effects of the latter on mtDNA integrity/content, we hypothesized that radical formation participates to EDAM. However, treatment with the mitochondrial ROS scavenger Mito-TEMPO gave contrasting findings. Indeed, while the scavenger reduced spinal cord ROS contents, prevented mtDNA reduction and counteracted the increase of cristae area, it was unable to affect alteration of mitochondrial transcriptome in immunized NOD mice undergoing EDAM. We consider these data of particular relevance. First, they provide the first indication that mitochondrial ROS play a role in the early events that precede onset of PEAE. Second, they corroborate our above-mentioned hypothesis that spinal cord changes in mtDNA and cristae morphology are functionally related. Third, if that would be the case, then mtDNA reduction likely occurs in axonal organelles. Lastly, the concomitant inability of Mito-TEMPO to restore expression of proteins involved in mitochondrial biogenesis and respiratory chain provides first hints of at least two independent signaling pathways participating to EDAM. Alternatively, EDAM represents a complex response where transcriptomic changes regulating mitochondrial homeostasis are upstream from ROS-dependent cristae remodeling.

The preset study is in line with a key role of mitochondria in PEAE pathogenesis, and also consistent with the ability of the bioenergetic boosting drug dexpramipexole to delay disease progression in PEAE NOD mice (Buonvicino et al., 2020).Overall, data disclose EDAM as a specific event in a mouse model of PMS, and suggest its involvement in pathogenesis of disease evolution. Understanding the underlying molecular mechanisms might help identifying innovative therapies to tackle MS progression.

CRediT authorship contribution statement

Daniela Buonvicino: Conceptualization, Methodology, Software,

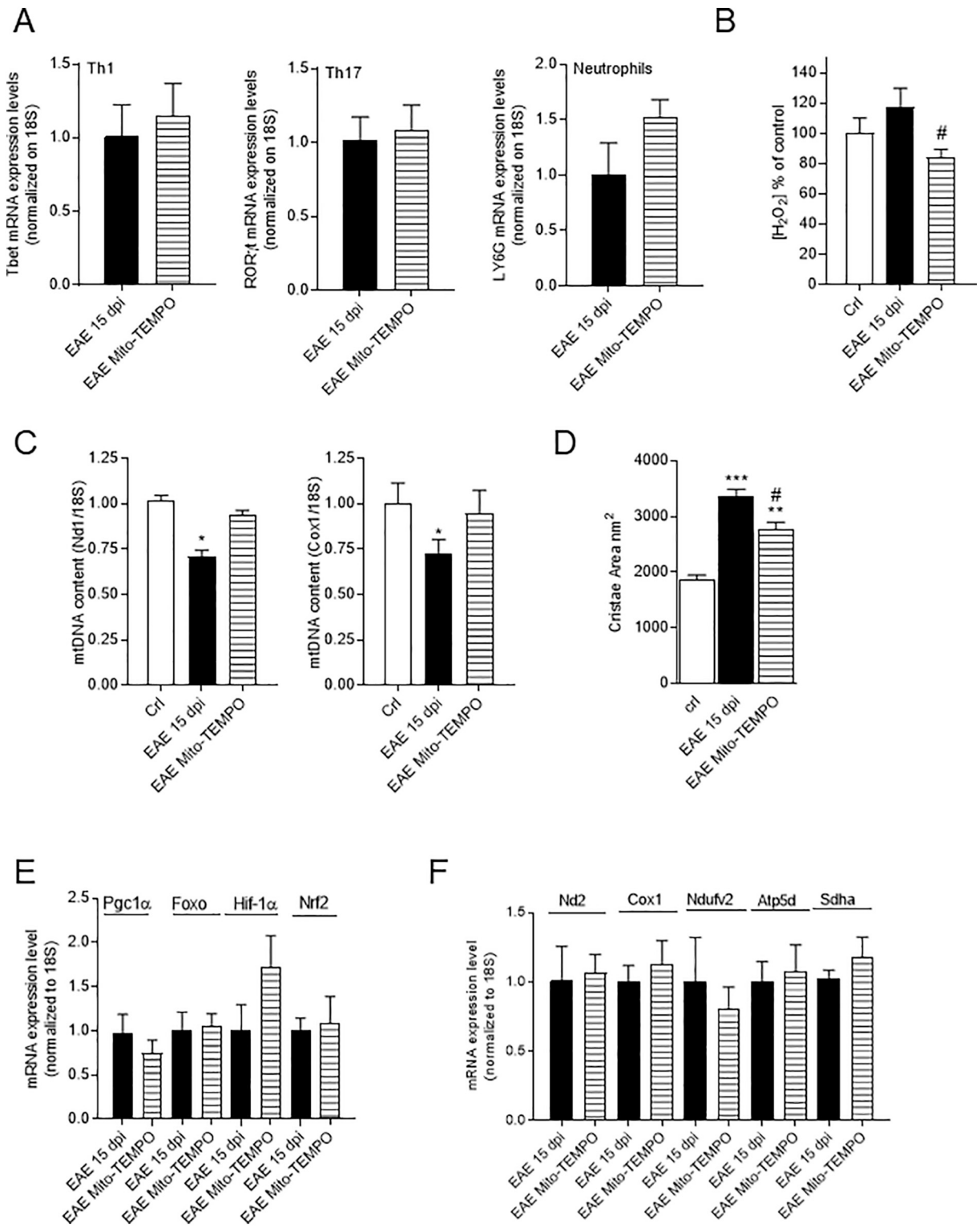

Fig. 8. Effects of Mito-TEMPO on mitochondrial parameters in the lumbar spinal cord of NOD mice after EAE induction.
Effects of daily administration of Mito-TEMPO (1 mg/kg i.p., from day of immunization) on immune infiltrates (A), H_2O_2 (100% equal 0.4 ± 0.03 μmol/l/mg tissue) (B) and mtDNA content (C) in the lumbar spinal cord NOD mice at day 15 post-immunization. In these animals, the effects of the treatment on cristae area of axonal mitochondria of lumbar spinal cord lateral columns are shown in (D). The effect of the treatment on mRNA levels of transcription factors Pgc1α, Foxo1, Nrf2 and Hif-1α (E), and respiratory complex subunits Ndufv2, Atp5d, Sdha, Cox1 and Nd2 (F) in the lumbar spinal cord lateral columns is shown. In (A-C) each column is the mean ± SEM of at least 5 mice per group. In (D) about 500 mitochondrial cristae areas belonging to control or immunized mice were measured. *$p < 0.05$, **$p < 0.01$ vs Crl, $^{\#}p < 0.05$ vs EAE (Student's t-test in A, E, F and ANOVA in B, C, D).

Validation, Formal analysis, Investigation, Data curation, Writing – original draft, Writing – review & editing, Visualization, Supervision, Project administration. **Giuseppe Ranieri:** Methodology, Software, Formal analysis, Validation, Data curation. **Daniele Guasti:** Methodology, Software, Data curation. **Alessandra Pistolesi:** Methodology, Formal analysis, Data curation. **Antonino Iurato La Rocca:** Methodology, Formal analysis, Data curation. **Elena Rapizzi:** Methodology, Software, Formal analysis, Data curation. **Alberto Chiarugi:** Conceptualization, Writing – original draft, Writing – review & editing, Supervision, Resources, Funding acquisition.

Declaration of Competing Interest

Authors declare no conflict of interest.

Data availability

Data will be made available on request.

Acknowledgments

This work was supported by grants from Italian Foundation for Multiple Sclerosis 2014/R/6 (recipient AC).

References

Alavi, M.V., Fuhrmann, N., 2013. Dominant optic atrophy, OPA1, and mitochondrial quality control: understanding mitochondrial network dynamics. Mol. Neurodegener. 8, 32. https://doi.org/10.1186/1750-1326-8-32.

Andrews, H., et al., 2006. Increased axonal mitochondrial activity as an adaptation to myelin deficiency in the Shiverer mouse. J. Neurosci. Res. 83, 1533–1539. https://doi.org/10.1002/JNR.20842.

Buonvicino, D., et al., 2018. Trigeminal ganglion transcriptome analysis in 2 rat models of medication-overuse headache reveals coherent and widespread induction of pronociceptive gene expression patterns. Pain 159, 1980–1988. https://doi.org/10.1097/j.pain.0000000000001291.

Buonvicino, D., et al., 2019. Neuroimmunological characterization of a mouse model of primary progressive experimental autoimmune encephalomyelitis and effects of immunosuppressive or neuroprotective strategies on disease evolution. Exp. Neurol. 322 https://doi.org/10.1016/J.EXPNEUROL.2019.113065.

Buonvicino, D., et al., 2020. Neuroprotection induced by dexpramipexole delays disease progression in a mouse model of progressive multiple sclerosis. Br. J. Pharmacol. 177, 3342–3356. https://doi.org/10.1111/BPH.15058.

Buonvicino, D., et al., 2021. Treatment with non-specific HDAC inhibitors administered after disease onset does not delay evolution in a mouse model of progressive multiple sclerosis. Neuroscience 465, 38–45. https://doi.org/10.1016/j.neuroscience.2021.04.002.

Burrows, D.J., et al., 2019. Animal models of multiple sclerosis: from rodents to zebrafish. Mult. Scler. 25, 306–324. https://doi.org/10.1177/1352458518805246.

Campbell, G., Mahad, D.J., 2018. Mitochondrial dysfunction and axon degeneration in progressive multiple sclerosis. FEBS Lett. https://doi.org/10.1002/1873-3468.13013.

Campbell, G.R., et al., 2014. The central role of mitochondria in axonal degeneration in multiple sclerosis. Mult. Scler. 20, 1806–1813. https://doi.org/10.1177/1352458514544537.

Cavone, L., et al., 2015. Dysregulation of sphingosine 1 phosphate receptor-1 (S1P1) signaling and regulatory lymphocyte-dependent immunosuppression in a model of post-fingolimod MS rebound. Brain Behav. Immun. 50, 78–86. https://doi.org/10.1016/J.BBI.2015.06.019.

D'Alise, A.M., et al., 2008. The defect in T-cell regulation in NOD mice is an effect on the T-cell effectors. Proc. Natl. Acad. Sci. U. S. A. 105, 19857–19862. https://doi.org/10.1073/PNAS.0810713105.

De Logu, F., et al., 2021. Peripheral nerve resident macrophages and Schwann cells mediate Cancer-induced pain. Cancer Res. 81, 3387–3401. https://doi.org/10.1158/0008-5472.CAN-20-3326.

Diaz, F., et al., 2005. Mice lacking COX10 in skeletal muscle recapitulate the phenotype of progressive mitochondrial myopathies associated with cytochrome c oxidase deficiency. Hum. Mol. Genet. 14, 2737–2748. https://doi.org/10.1093/HMG/DDI307.

Dikalova, A.E., et al., 2010. Therapeutic targeting of mitochondrial superoxide in hypertension. Circ. Res. 107, 106–116. https://doi.org/10.1161/CIRCRESAHA.109.214601.

Felici, R., et al., 2017. Post onset, oral rapamycin treatment delays development of mitochondrial encephalopathy only at supramaximal doses. Neuropharmacology 117, 74–84. https://doi.org/10.1016/J.NEUROPHARM.2017.01.039.

Filograna, R., et al., 2021. Mitochondrial DNA copy number in human disease: the more the better? FEBS Lett. 595, 976–1002. https://doi.org/10.1002/1873-3468.14021.

Galber, C., et al., 2021. The f subunit of human ATP synthase is essential for normal mitochondrial morphology and permeability transition. Cell Rep. 35 https://doi.org/10.1016/J.CELREP.2021.109111.

James, C.R., et al., 2016. Reduced interleukin-2 responsiveness impairs the ability of Treg cells to compete for IL-2 in nonobese diabetic mice. Immunol. Cell Biol. 94, 509–519. https://doi.org/10.1038/ICB.2016.7.

Kondadi, A.K., et al., 2019. Functional interplay between cristae biogenesis, mitochondrial dynamics and mitochondrial DNA integrity. Int. J. Mol. Sci. https://doi.org/10.3390/ijms20174311.

Kondadi, A.K., et al., 2020. Cristae membrane dynamics - a paradigm change. Trends Cell Biol. 30, 923–936. https://doi.org/10.1016/J.TCB.2020.08.008.

Kummari, E., et al., 2019. Neuroinflammation and B-cell phenotypes in cervical and lumbosacral regions of the spinal cord in experimental autoimmune encephalomyelitis in the absence of pertussis toxin. Neuroimmunomodulation 26, 198–207. https://doi.org/10.1159/000501765.

Ladakis, D.C., et al., 2022. Mitochondrial measures in neuronally enriched extracellular vesicles predict brain and retinal atrophy in multiple sclerosis. Mult. Scler. J. 28, 2020–2026. https://doi.org/10.1177/13524585221106290.

Landucci, E., et al., 2021. Neuroprotective effects of thymoquinone by the modulation of ER stress and apoptotic pathway in in vitro model of excitotoxicity. Molecules 26, 1592. https://doi.org/10.3390/molecules26061592.

Lee, A.R., et al., 2019. Involvement of mitochondrial biogenesis during the differentiation of human periosteum-derived mesenchymal stem cells into adipocytes, chondrocytes and osteocytes. Arch. Pharm. Res. 42, 1052–1062. https://doi.org/10.1007/S12272-019-01198-X.

Liang, H.L., et al., 2010. SOD1 and MitoTEMPO partially prevent mitochondrial permeability transition pore opening, necrosis, and mitochondrial apoptosis after ATP depletion recovery. Free Radic. Biol. Med. 49, 1550–1560. https://doi.org/10.1016/J.FREERADBIOMED.2010.08.018.

Liu, Y., et al., 2018. Mito-TEMPO alleviates renal fibrosis by reducing inflammation, mitochondrial dysfunction, and endoplasmic reticulum stress. Oxidative Med. Cell. Longev. 2018 https://doi.org/10.1155/2018/5828120.

Moraes, C.T., 2001. What regulates mitochondrial DNA copy number in animal cells? Trends Genet. 17, 199–205. https://doi.org/10.1016/S0168-9525(01)02238-7.

Palumbo, S., Pellegrini, S., 2017. Experimental in vivo models of multiple sclerosis: state of the art. In: Multiple Sclerosis: Perspectives in Treatment and Pathogenesis. Codon Publications, pp. 173–183. https://doi.org/10.15586/codon.multiplesclerosis.2017.ch11.

Peiris, M., et al., 2007. A model of experimental autoimmune encephalomyelitis (EAE) in C57BL/6 mice for the characterisation of intervention therapies. J. Neurosci. Methods 163, 245–254. https://doi.org/10.1016/J.JNEUMETH.2007.03.013.

Perkins, G.A., Ellisman, M.H., 2011. Mitochondrial configurations in peripheral nerve suggest differential ATP production. J. Struct. Biol. 173, 117–127. https://doi.org/10.1016/J.JSB.2010.06.017.

Picca, A., et al., 2020. Mitochondrial dysfunction, oxidative stress, and neuroinflammation: intertwined roads to neurodegeneration. Antioxidants (Basel, Switzerland) 9, 1–21. https://doi.org/10.3390/ANTIOX9080647.

Pöllinger, B., et al., 2009. Spontaneous relapsing-remitting EAE in the SJL/J mouse: MOG-reactive transgenic T cells recruit endogenous MOG-specific B cells. J. Exp. Med. 206, 1303–1316. https://doi.org/10.1084/JEM.20090299.

Rapizzi, E., et al., 2012. Mitochondrial function and content in pheochromocytoma/paraganglioma of succinate dehydrogenase mutation carriers. Endocr. Relat. Cancer 19, 261–269. https://doi.org/10.1530/ERC-11-0263.

Rosenkranz, S.C., et al., 2021. Enhancing mitochondrial activity in neurons protects against neurodegeneration in a mouse model of multiple sclerosis. Elife 10, 1–60. https://doi.org/10.7554/ELIFE.61798.

Schattling, B., et al., 2019. Bassoon proteinopathy drives neurodegeneration in multiple sclerosis. Nat. Neurosci. 22, 887–896. https://doi.org/10.1038/S41593-019-0385-4.

Shetty, S., et al., 2021. Mitochondria-targeted antioxidant, Mito-TEMPO mitigates initiation phase of N-Nitrosodiethylamine-induced hepatocarcinogenesis. Mitochondrion 58, 123–130. https://doi.org/10.1016/J.MITO.2021.03.001.

Sogl, B., et al., 2000. Biogenesis of giant mitochondria during insect flight muscle development in the locust, Locusta migratoria (L.). transcription, translation and copy number of mitochondrial DNA. Eur. J. Biochem. 267, 11–17. https://doi.org/10.1046/J.1432-1327.2000.00936.X.

Wang, Y., et al., 2019. Mitochondrial dysfunction in neurodegenerative diseases and the potential countermeasure. CNS Neurosci. Ther. 25, 816–824. https://doi.org/10.1111/CNS.13116.